J. Fluid Mech. (1997), *vol.* 339, *pp.* 143–172

Copyright © 1997 Cambridge University Press

Deformable roll coating flows: steady state and linear perturbation analysis

By MARCIO S. CARVALHO† AND L. E. SCRIVEN

Center for Interfacial Engineering and Department of Chemical Engineering and Materials Science, University of Minnesota, Minneapolis, MN 55455, USA

(Received 22 November 1995 and in revised form 16 December 1996)

Roll coating is distinguished by the use of one or more gaps between rotating cylinders to meter a continuous liquid layer and to apply it to a continuous flexible substrate. Of the two rolls that make a forward or reverse roll coating gap, one is often covered by a layer of more-or-less deformable elastomer. Liquid carried into the converging side of the nip can develop high enough pressure to deform the resilient cover, which changes the nip profile and thus alters the velocity and pressure field. This elastohydrodynamic coupled action is not yet well understood. Theoretical modelling has to take into account the viscous flow, the roll deformation and the free-surface effects in order to predict the flow behaviour.

In this work the flow between a rigid and a deformable counter-rotating roll that shares the same angular speed is described by the lubrication approximation together with a viscocapillary model, based in the film-flow equation, for the film-split region. The deformation of the elastomer layer is modelled by Hookean springs oriented radially, which constitute a one-dimensional model. The stability of the system to transverse perturbation is analysed by examining the time-dependent response to infinitesimal disturbances in order to identify those that grow fastest.

The corresponding system of equations is solved by Newton's method with first-order continuation. The relationship between coating thickness, operational parameters (loading force, gap setting, roll velocities, etc.), liquid properties and the properties of the cover is reported, as well as the critical capillary number for onset of ribbing and wavelengths of the ribbing pattern predicted by the mathematical model. The results indicate how a deformable cover may be used in order to delay the onset of ribbing for a desired coating thickness.

In order to validate the theoretical predictions of the viscocapillary/Hookean spring model, the symmetric film-split flows between a pair of rigid rolls and a pair consisting of a deformable roll and a rigid one were also analysed experimentally.

1. Introduction

Roll coating is distinguished by the use of one or more gaps between rotating cylinders to meter a continuous liquid layer and to apply it to a continuous flexible substrate called a web. The metering and application functions can be performed in gaps between counter-rotating cylinders, which is called forward roll action, or between co-rotating ones, which is called reverse roll action. This paper deals with forward roll action. Figure 1 sketches examples of three-roll and four-roll coaters.

† Present address: Imation Corporation, 3M Center, 235-BF-19, St.Paul, MN, 55144, USA.

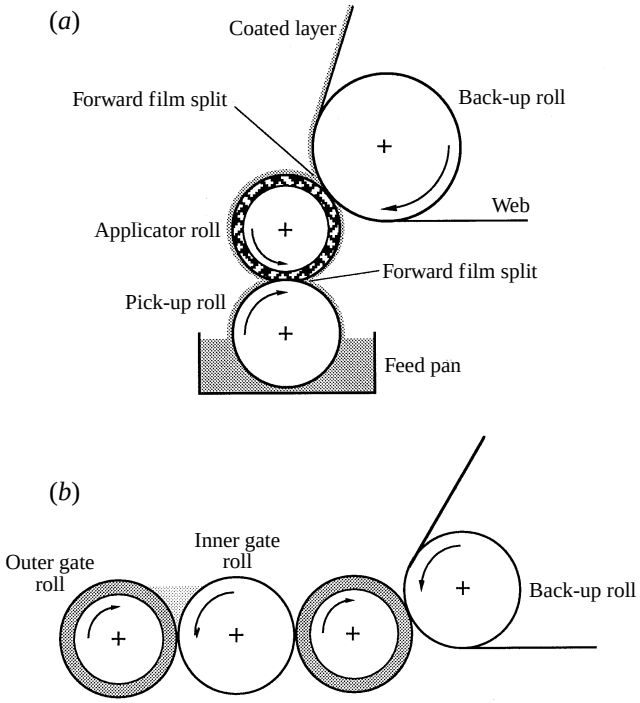

FIGURE 1. Examples of forward roll coaters. (*a*) Three-roll transfer coater with feed pan. (*b*) Four-roll transfer coater with feed pond.

Despite the wide variety of roll coating systems, each of them can be broken into similar parts, as was mentioned by Coyle, Macosko & Scriven (1986) and developed by Benjamin, Anderson & Scriven (1995). In order to understand the whole operation, one needs to understand first individual flows between pairs of rolls in both the forward and reverse modes. Benjamin *et al.* (1995) used simple mass balances to combine the information derived from the analysis of these *unit flows* between each pair of rolls to relate the thickness of the delivered layer, or the coat weight, to separation, speed ratio and roll radii of each roll pair.

The flows between pairs of rotating rigid rolls have been extensively studied. When the roll radii are much larger than the distance between the roll surfaces, as is often true, the flow in the gap region is nearly rectilinear and the governing Navier–Stokes system, or its modification for shear-sensitive liquids, is well approximated by lubrication theory, at least far enough from the menisci upstream and downstream. With this approximation Greener & Middleman (1975) analysed flows of Newtonian and non-Newtonian power-law liquids between rolls of equal radii and speeds in the forward roll mode. However, downstream from the region of closest approach between the rolls, the liquid splits into two films, one attached to each roll. Near this film split meniscus, the flow field is two-dimensional and bounded by a free surface. Accurately describing it requires solving the complete Navier–Stokes system. Nevertheless, a common approach has been to proceed with the lubrication approximation and adopt a plausible boundary condition at the film split meniscus.

Several options appear in the literature. The first and simplest choice is to set both the pressure and the pressure gradient to zero at the film-split meniscus. This condition is known as *Reynolds' boundary condition*, and it is the least accurate of the available

boundary conditions used at the film-split free surface. A natural improvement is to set the pressure at the film-split to be subambient, due to the capillary pressure jump associated with the meniscus curvature. An extra equation is still needed to locate the position of the meniscus. A condition postulated by Hopkins (1957), and used by Savage (1977*a*), is to locate the film-split meniscus at the first stagnation line (point in a cross-section) downstream of the plane through the centres of the rolls and midway between the roll surfaces. Coyle *et al.* (1986) extended this idea to the asymmetric case, postulating that the film-split line is located at the point at which both the velocity and its derivative in the direction perpendicular to the flow vanish. This condition does not locate a stagnation line, except in the symmetric situation or when one of the rolls is stationary. Savage *et al.* (1992) modified Coyle's approach and instead located the film-split meniscus at the first stagnation line, i.e. at the point at which both velocity components vanish. This leads to a relation between film thickness ratio and roll speed ratio that is close, in some of the range, to solutions of the full Navier–Stokes system. A different approach was adopted by Savage (1977*a*) and later by Fall (1985) to set the film split boundary condition. They used the results reported by Coyne & Elrod (1970), that solved approximately the Navier–Stokes system of equations near the meniscus. The predictions obtained with the lubrication approximation with Hopkin's boundary condition, the full Navier–Stokes system (solved by Galerkin's method and finite element basis functions), and an asymptotic expansion of the Navier–Stokes system appropriate when the gap is much less than the roll diameter were compared by Coyle *et al.* (1986). They found that the lubrication model is accurate only at high capillary number (the product of mean roll speed and viscosity divided by surface tension), where the effect of surface tension is weak. The lubrication model is inaccurate when the effect is strong, i.e. low capillary number, because the *ad hoc* boundary condition does not adequately represent the capillary pressure gradient induced by the meniscus curvature in the film-split region and the accompanying two-dimensional flow.

Kubota & Scriven (1993) employed what is called a viscocapillary model to describe film-splitting flow: the flow near the meniscus is approximated by the Deryagen & Levi (1959) modification of the Laudau–Levich equation of the flow carried out of a pool by a roll that dips into it, i.e. a dip-coating flow, and elsewhere the flow is approximated by lubrication flow.

In practice, rigid gaps, i.e. pairs of rigid rolls, are rare in roll systems, except in reverse roll metering and meniscus coating (Gaskell *et al.* 1995). Usually one of the rolls is covered with a resilient layer that deforms during operation, as shown in figure 1. The main purposes of using a deformable roll cover are: (i) to avoid the risk of clashing two hard rolls (typically made of steel); (ii) to obtain much thinner films than ordinarily can be achieved by rigid roll coating; (iii) to reduce or delay the onset of the ribbing defect; and (iv) to transfer an already metered film (wipe roll coating). The use of deformable rolls is not restricted to roll coating methods. In die coating, a die is pressed against a rubber-covered backup roll. A very narrow gap is formed and shear rates of the order of 10^5 s^{-1} can occur, drastically reducing the viscosity of the liquid if it has a shear-thinning behaviour.

The deformation of the roll cover alters the shape of the boundaries of the coating flow. That flow generates pressure and viscous stresses that in turn affect the deformation of the roll cover. Hence the viscous liquid flow between the rolls and the elastic deformation of the roll cover are coupled in what is called elastohydrodynamic behaviour. How this behaviour depends on the thickness and properties of the roll cover, and how it influences wet coating thickness (which translates to 'coat weight')

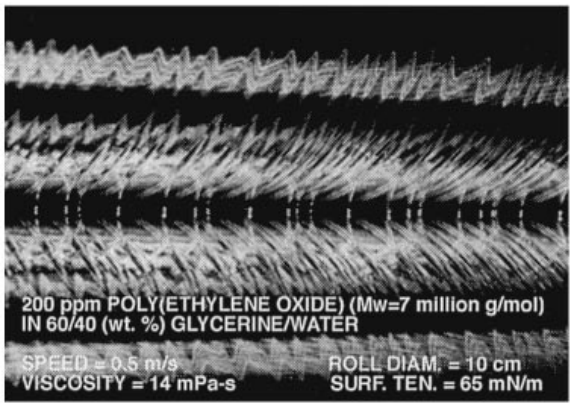

FIGURE 2. Ribbing instability in a forward roll coating gap. The field of view is approximately 10 cm wide.

versus roll loading and roll speeds, and how it affects crossweb and downweb coating uniformity and roll drag are not yet completely understood.

Analysis of flows between a rigid and a deformable roll is rare. Coyle (1988) launched an analysis by using the lubrication approximation to describe the flow field and an array of independent linear one-dimensional radial elements to describe the elastic rubber deformation. The effect of the free surfaces of the liquid was not taken into account in his work. The coupling between solid deformation and liquid flow also occurs in the elastohydrodynamic lubrication of bearings. The fundamentals of this area have been well established, especially by Dowson & Higginson (1966).

Carvalho & Scriven (1994*a*) took up Coyle's analysis and examined the differences between the use of a one-dimensional linearly elastic model and a one-dimensional nonlinearly elastic model that better describes the response of rubber when deformation is appreciable. They also explored the use of a two-dimensional plane-strain approximation, that accounts for the Poisson's ratio of the rubber. The approach did not take into account the thickness of the elastic layer. The deformation of the roll surface was derived from that of an elastic half-space. Both models were found to predict the same trends and in the cases examined the flow rates differed by no more than 10%. The most important conclusion of the comparisons is that the one-dimensional model, although much simpler, predicts fairly well the overall performance of forward roll action in a deformable gap.

Although the location of the film split and the stability of the flow with respect to transverse disturbances is strongly affected by capillary number, surface tension effects were not consider by either Coyle (1988) or Carvalho & Scriven (1994*a*).

The first part of this paper describes the analysis of a forward deformable roll gap, with rolls sharing the same angular speed, by means of a viscocapillary model, i.e. the lubrication approximation for most of the flow and a flow with capillary pressure gradient as described by the film flow equation of Deryagen & Levi (1959) in the film-split region, together with a one-dimensional elastic radial elements of the resilient roll cover.

One of the drawbacks of forward roll coating gaps is that, at high speeds, the liquid layer on each of the roll surfaces has a wavy thickness profile in the transverse direction, a pattern commonly called *ribbing* and also known as *corduroy* and *pin-striping* (see figure 2). In the second part of this paper, the stability of the flows

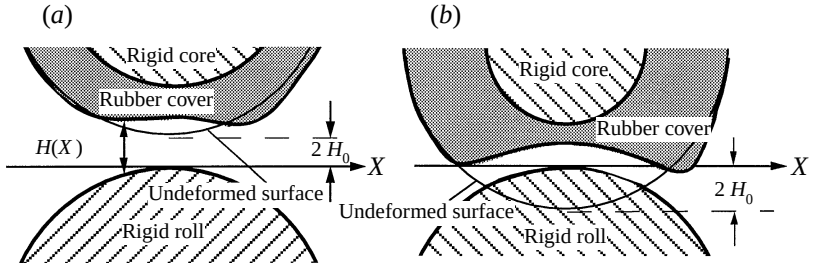

FIGURE 3. Gap profile with deformable roll. (*a*) Positive gap, i.e. clearance between undeformed rolls. (*b*) Negative gap, i.e. interference between undeformed rolls. The parameter H_0 has different meanings in the two situations.

obtained with the viscocapillary model to transverse perturbation is analysed by examining the time-dependent response to infinitesimal disturbances in order to identify those that grow fastest, following Fall's (1985) approach, but here including the roll deformation and a better description of the flow near the meniscus. The goal is to understand the effect of the roll cover deformation on the onset of ribbing. The predicted critical capillary number, and the wavelengths of the ribbing pattern are compared with values obtained from experiments.

2. Mathematical formulation of the base flow

Each gap in a forward roll coater can be operated two ways. One is to keep the axes of the two rolls parallel, with one axis fixed and the other movable in response to externally imposed loading (usually reported as force per unit length). The gap takes the value at which the integrated traction of the liquid on the movable roll equals the loading. If one of the rolls is deformable, then to each loading there corresponds not only a centre-to-centre distance between the rolls, but also a roll deformation and a gap profile that depends on that deformation. This is called *load-controlled*, or *force-controlled operation*. The other way is to fix the axes of both rolls. This is called *fixed-gap operation*. Actually there are intermediate ways in which the loading is a function of the centre-to-centre distance, as when the movable roll is loaded by springs or equivalents. This is called *compliant-loading operation*.

When the centre-to-centre distance is greater than the sum of the roll radii, the rolls do not intersect each other when they are undeformed: there is a *positive gap* (Coyle 1988), as in figure 3(*a*). When the centre-to-centre distance is less than the sum of the roll radii, the rolls necessarily would intersect each other were they undeformed: there is a *negative gap*, or *nip*, as in figure 3(*b*). In a force-controlled operation, a small enough loading yields a positive gap, whereas a large enough loading produces a negative gap. In this paper, only positive gaps are considered.

In analysing roll coater gaps it is convenient to suppose that the centre-to-centre distance between the rolls of a pair is set, and to evaluate the loading required to maintain that distance. This tactic is used here, but in no way limits the results to fixed-gap operation.

2.1. *Lubrication approximation*

In flows where the particle paths (streamlines in the steady-state problem) are almost parallel, scaling arguments can be used to simplify the Navier–Stokes equation to an ordinary differential equation for pressure that captures the most important features

of the problem. In most of the gap region, the lubrication approximation is valid and the pressure distribution is given by (cf. Cameron 1966)

$$\frac{\mathrm{d}P}{\mathrm{d}X} = \frac{12\mu}{H(X)^3}\Big[\overline{V}H(X) - Q\Big], \tag{1}$$

where X is the distance along the gap from the plane through the two roll axes, $\overline{V} \equiv (V_A + V_B)/2$ is the average surface velocity of the rolls, V_A being the surface velocity of the one (upper roll in figure 3) which is taken to be deformable, and V_B being the surface velocity of the other (lower roll in figure 3) which is not deformable. The average surface velocity is related to the speed ratio $S \equiv V_A/V_B$ by

$$\overline{V} = \tfrac{1}{2}(S+1)V_B.$$

$S > 0$ describes forward roll action and $S < 0$ reverse roll action. $S = 0$ amounts to a stationary but deformable wiper bar. $H(X) \equiv H_A(X) - H_B(X)$ is the local clearance between the roll surfaces, H_A and H_B being the respective distances from a reference plane $Y = 0$ that is tangent to the rigid roll and perpendicular to the plane through the axes (figure 3). Q is the flow rate of liquid through the gap per unit length of the rolls.

The circular profiles of the undeformed roll surfaces are conveniently and well approximated by arcs of parabola. For the positive gap case (figure 3(a)), the expressions are

$$H_A(X) = 2H_0 + R_A - (R_A^2 - X^2)^{1/2} + D(X) \approx 2H_0 + \frac{X^2}{2R_A} + D(X),$$

$$H_B(X) = -R_B + (R_B^2 - X^2)^{1/2} \approx -\frac{X^2}{2R_B}.$$

It follows that the local clearance is

$$H(X) \equiv H_A(X) - H_B(X) = 2H_0 + \frac{X^2}{R} + D(X). \tag{2}$$

$2\,H_0$ is the clearance between the undeformed rolls. $D(X)$ is the local displacement of the deformable roll surface in the direction parallel to the plane through the roll axes. The local displacement is related to the local pressure in the flowing liquid by a constitutive equation. R is the effective radius of the two rolls:

$$\frac{1}{R} \equiv \frac{1}{2}\left(\frac{1}{R_A} + \frac{1}{R_B}\right).$$

Two boundary conditions are needed in order to integrate (1). A common approach is to disregard the feed condition and suppose that it is far enough from the gap plane that the pressure is substantially atmospheric upstream at the inlet boundary:

$$P(-\infty) = 0. \tag{3}$$

If the free-surface effects downstream are taken into account, the pressure at the film meniscus is subambient, due to the capillary pressure jump associated with the meniscus curvature:

$$P(X_m) = -\frac{\sigma}{R_m}. \tag{4}$$

This introduces two more unknowns: the radius of curvature of the meniscus R_m and the position of the film split X_m. Two more conditions at the downstream

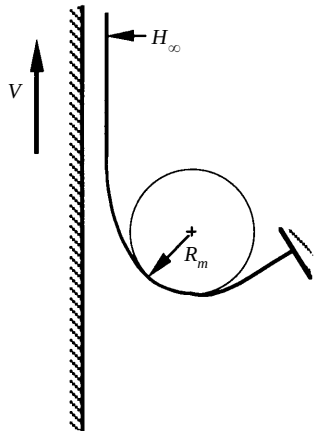

FIGURE 4. Dip coating from a quiescent pool with a meniscus-limiting obtruction. R_m is the radius of curvature of the meniscus.

boundary are needed in order to close the system of equations. Different choices, reviewed in the introduction section, are available in the literature.

If the capillary number is small, i.e. the effect of surface tension is strong, there is a recirculation attached to the film-split meniscus and the first stagnation point is not located at the free surface, invalidating the assumption of some of the models described in the introduction. Here, the equation that describes the film flow entrained by a solid surface moving in its own plane and out of a virtually quiescent liquid pool, as in a dip-coating operation, is used at the film-split boundary to complete the formulation of the problem.

2.2. *Viscocapillary model*

The dragging of liquid out of a pool by an ascending solid surface was first analysed by Landau & Levich (1942); cf. figure 4. They found the final film thickness by solving a film profile equation that approximates, in the manner of matched asymptotic expansions, the local balances of viscous, gravity, capillary, and pressure forces along the emerging film. Later Deryagin & Levi (1959) specialized the analysis to the simpler case of a pool whose free surface is narrow and curved enough to make the effect of gravity negligible compared to that of the capillary pressure induced by the action of surface tension in the curved surface. Their relation between the final layer thickness H_∞ and the radius of curvature R_m of the meniscus of the virtually quiescent liquid is

$$H_\infty = 1.34\ R_m\ Ca^{2/3}, \qquad Ca \equiv \mu V/\sigma.$$

Ca is the capillary number, σ is the liquid surface tension, μ is the liquid viscosity and V is the plate velocity. This specialization of the Landau–Levich equation is often given the same name. The Landau–Levich equation is strictly valid at low capillary number ($Ca \ll 1$).

Because the liquid immediately under the middle of the film-split meniscus moves relatively slowly and the dominant forces in the layers being drawn from it by the two rolls are viscous drag and capillary pressure, the flow in the film-split region resembles the one encounter when a plate drags a liquid out of a pool. This approach was first used by Kubota & Scriven (1993), and later by Carvalho & Scriven (1994*b*) and Gaskell *et al.* (1995). The final layer thickness on each roll can be approximated

by the Landau–Levich equation:

$$H_A = 1.34\ Ca^{2/3}\left(\frac{2S}{S+1}\right)^{2/3} R_m \quad \text{and} \quad H_B = 1.34\ Ca^{2/3}\left(\frac{2}{S+1}\right)^{2/3} R_m. \tag{5}$$

The capillary number Ca is defined in terms of the average roll speed $\overline{V}$, i.e. $Ca \equiv \mu\overline{V}/\sigma$. Balancing inflow and outflow leads to

$$\frac{Q}{2\overline{V}}(1+S) = S\ H_A + H_B. \tag{6}$$

Q is the total flow rate through the gap. Equations (5) and (6) can be rearranged as

$$H_A = \frac{Q}{2\overline{V}}\frac{(S+1)S^{2/3}}{1+S^{5/3}}, \qquad H_B = \frac{Q}{2\overline{V}}\frac{(S+1)}{1+S^{5/3}}, \tag{7}$$

$$R_m = \frac{1}{1.34\ Ca^{2/3}}\frac{Q}{2\overline{V}}\frac{(S+1)}{1+S^{5/3}}\left(\frac{S+1}{2}\right)^{2/3}. \tag{8}$$

Thus the layer thickness on each roll is a function only of the flow rate Q and roll speeds.

The ratio of layer thicknesses, or film-thickness ratio, as a function of the speed ratio follows naturally from (7):

$$\frac{H_A}{H_B} = \left(\frac{V_A}{V_B}\right)^{2/3}.$$

The 2/3 power-law dependence accords well with the solution of the full Navier–Stokes system at vanishing Reynolds and Stokes numbers (Coyle *et al.* 1986). The film-split position X_m is dictated by geometric requirements. If the meniscus is simply modelled as an arc of circle that is tangent to uniform films where it joins them, as Greener & Middleman (1975) took it to be, the meniscus coordinate X_m is given by

$$H(X_m) = H_A + H_B + 2R_m.$$

However, from the film-split position to the uniform layer downstream, the curvature of the meniscus gradually changes, as indicated in figure 5. Kubota & Scriven (1993) matched a meniscus of constant curvature with the asymptotic solution of the equation of film flow on a rising plate, instead of with uniform films. They found that this expedient improved the agreement of the viscocapillary model with the Navier–Stokes solution at higher capillary numbers. In their scheme, the position X_m of the film split is obtained from (refer to figure 5)

$$H(X_m) = K(H_A + H_B) + R_m(\cos\theta_A + \cos\theta_B).$$

K, θ_A and θ_B are evaluated with formulas from the asymptotic solution of the film profile equation:

$$K = 1.644,$$

$$\theta_A = \arctan\left\{-0.644\left(\frac{6CaS}{S+1}\right)^{1/3}\right\}, \quad \theta_B = \arctan\left\{-0.644\left(\frac{6Ca}{S+1}\right)^{1/3}\right\}.$$

Replacing these constants and the film thickness expressions (7), and using the local

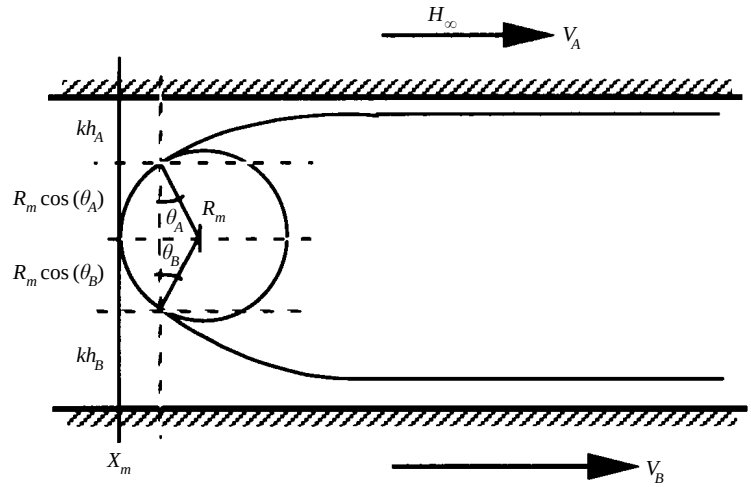

FIGURE 5. Sketch of film-split meniscus. The curvature of the meniscus gradually changes from a constant curvature to a plane film.

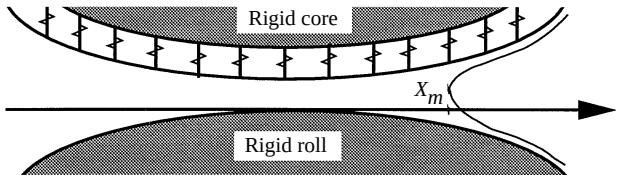

FIGURE 6. Sketch of one-dimensional spring model of the rubber cover on a rigid core opposite a rigid roll.

clearance (2) yields the meniscus position X_m:

$$H(X_m) = 2H_0 + \frac{X_m^2}{R} + D(X_m) = 1.644\frac{Q}{2\overline{V}}\frac{1+S}{1+S^{5/3}}(1+S^{2/3}) + R_m\left\{\frac{1}{1+0.414(6CaS/(1+S))^{2/3}} + \frac{1}{1+0.414(6Ca/(1+S))^{2/3}}\right\}. \quad (9)$$

In sum, the boundary conditions on (1) are the pressure imposed at the inlet (3), the pressure imposed at the film split, the capillary pressure jump (4), the radius of curvature (8), and the geometric relation (9). In order to integrate (1), the displacement of the soft roll $D(X)$ has to be related to the pressure distribution $P(X)$. We chose for the present purpose the one-dimensional elastic spring model, that is described next.

2.3. *One-dimensional Hookean model*

One-dimensional models amount to a continuous distribution of parallel independent springs. A discrete analogue is diagrammed in figure 6. The deformation at each spring depends solely on the pressure at its terminus in the roll surface.

Such a model represents neither shear stresses in the roll cover nor its incompressibility. Consequently, it does not account for the contributions to deformation at one place on the surface by pressures acting at others. The Hookean version, which was

used by Coyle (1988), makes the local displacement directly proportional to the local pressure:

$$D(X) = \frac{1}{K} P(X). \tag{10}$$

The spring constant K is related to the roll cover properties: elastic modulus E, Poisson's ratio v, and thickness L.

Dowson & Jin (1989) used a similar approach, called the constrained column model. Johnson (1985) showed that the spring constant K strongly depends on the values of Poisson's ratio and that the model does not formally apply for incompressible materials, i.e. $v = 0.5$. As Poisson's ratio approaches 0.5, the spring constant grows unbounded and the deformation at each point tends to zero. At vanishing Poisson's ratio ($v = 0$), the spring constant is simply $K = E/L$. In general, $K = \alpha E/L$, where α is a function of Poisson's ratio.

Dowson & Jin (1989) showed that the one-dimensional model (constrained-column model) can be applied to predict elastic deformation if Poisson's ratio is less than 0.45 and the ratio of the loading width to the deformable layer thickness is greater than 2.

In most applications of deformation roll coating, the length of the bead (loading width) is greater than twice the roll cover thickness. Although most materials used in roll cover have high Poisson's ratio (close to 0.5), at which the one-dimensional spring model does not formally apply, it gives an approximation of the overall behaviour of the incompressible roll cover.

2.4. *Solution of the equation system*

In order to solve the equations most efficiently, appropriate units have to be chosen for the variables and the equations thereby written in dimensionless form. Accordingly

$$x \equiv \frac{X}{(RH_0)^{1/2}}, \quad h(x) \equiv \frac{H(X)}{H_0}, \quad d(x) \equiv \frac{D(X)}{H_0}, \quad q \equiv \frac{Q}{2\overline{V}H_0}, \quad p_v \equiv \frac{PH_0}{\mu\overline{V}}\left(\frac{H_0}{R}\right)^{1/2}.$$

The equation system in dimensionless form becomes

$$\frac{\mathrm{d}p_v}{\mathrm{d}x} = \frac{12}{[h(x)]^2} - \frac{24q}{[h(x)]^3}, \tag{11a}$$

$$p_v(-\infty) = 0, \tag{11b}$$

$$p_v(x_m) = -\frac{1}{Ca(R/H_0)^{1/2} r_m}, \tag{11c}$$

$$r_m = \frac{1}{1.34Ca^{2/3}} q \frac{1+S}{1+S^{5/3}} \left(\frac{1+S}{2}\right)^{2/3}, \tag{11d}$$

$$h(x_m) = 1.644q\frac{1+S}{1+S^{5/3}}(1+S^{2/3}) + r_m\left\{\frac{1}{(1+0.414(6CaS/(1+S))^{2/3})} + \frac{1}{(1+0.414(6Ca/(1+S))^{2/3})}\right\}, \tag{11e}$$

$$h(x) = 2 + x^2 + d(x), \tag{11f}$$

$$d(x) = Ne\ p_v(x). \tag{11g}$$

The solution of the equation system obtained depends on: the dimensionless gap H_0/R; the capillary number Ca; the speed ratio S; and the modified elasticity

number *Ne*. The latter measures the relative magnitudes of the liquid pressure, which is proportional to viscosity and average roll speed, and elastic stress in the roll cover, which is proportional to the empirical spring constant K:

$$Ne \equiv \frac{\mu \overline{V}}{K R^2} \left(\frac{R}{H_0} \right)^{5/2}.$$

In this formulation, the elementary elasticity number $Es \equiv \mu \overline{V}/K R^2$ appears only in combination with H_0/R.

The equation system (11) was solved by using a finite difference formula to approximate the pressure derivative. The domain was divided into n intervals by $n+1$ nodes (equal intervals would be convenient, but suitably unequal ones proved more efficient: see below). The values of pressure, displacement and coordinate at each of the nodes except the inflow boundary, together with the flow rate, were the unknowns.

The position of the inflow boundary was so chosen that the flow rate was insensitive to locating it any further upstream.

The resulting algebraic system of equations, $3n + 1$ in number, is nonlinear. To solve this system, Picard iteration would be simple: evaluate the pressure profile with the values of the displacements (roll profile) from the previous iteration; with the new pressure profile evaluate the new displacement distribution; and so on. As the literature about this procedure in elastohydrodynamics testifies (Dowson & Higginson 1966), it is generally slow to converge if it converges at all.

The method of choice for this type of problem is Newton's method, which requires evaluation of the full Jacobian matrix, i.e.

$$\boldsymbol{u}_{(n+1)} = \boldsymbol{u}_{(n)} + \Delta \boldsymbol{u}; \quad \boldsymbol{J}(\Delta \boldsymbol{u}) = -\boldsymbol{R}.$$

$\boldsymbol{u}$ is the vector of unknowns, $\boldsymbol{R}$ is the vector of residuals of the discretized equations, and $\boldsymbol{J}$ is the Jacobian matrix. The entries of the Jacobian are the sensitivities of the residuals to the unknowns, i.e.

$$J_{ij} \equiv \frac{\partial R_i}{\partial u_j}.$$

The initial approximation in Newton's method was determined by first-order continuation in the parameter space, i.e. it was evaluated from the previous solution and the latter's sensitivity to whichever parameter ξ, e.g. capillary number or elasticity number, was being changed:

$$\boldsymbol{u}_{(0)}(\xi_{i+1}) = \boldsymbol{u}(\xi_i) + \frac{\partial \boldsymbol{u}}{\partial \xi} \Delta \xi, \quad \boldsymbol{J} \left(\frac{\partial \boldsymbol{u}}{\partial \xi} \right) = -\frac{\partial \boldsymbol{R}}{\partial \xi}.$$

By controlling the step size by which the parameter was changed, convergence was achieved within 3 to 5 iterations and was generally at the quadratic rate expected of Newton iteration as the solution is approached. In the range of parameters explored, $n = 600$ intervals sufficed; increasing n to 800 altered the flow rate and film-split location by less than 0.1%.

The Jacobian matrix was stored in a compressed sparse row format and at each Newton iteration the system of linear equations was solved by the GMRES iterative algorithm with preconditioning (Saad & Schultz 1986). Only at the first Newton step was a preconditioner matrix evaluated; what was employed was an incomplete LU factorization (Saad & Schultz 1986) of the Jacobian matrix. The same preconditioner was used in the subsequent Newton steps. This saved a lot of computing time, because at each parameter continuation step, only one Gauss elimination (incomplete) was

performed. The dimension of the Krylov subspace used in GMRES was fixed at 10. The total computing time (CPU time) did not seem to diminish with the use of a larger subspace. A representative run consumed approximately 7 s in a Hewlett-Packard workstation, series 735.

The pressure distribution of roll coating flows has regions of steep gradient and others of high curvature. In order to reduce the error of approximating the solution by finite differencing, the number of uniformly spaced nodes needed in some extreme cases would be very large. This was avoided by using the continuation-adaptive strategy explained by Benner, Davis & Scriven (1987). The nodes were relocated as the parameters were changed in continuation in such a way that they concentrate in regions where the pressure profile was steep or highly curved. The weighting function chosen as the means of distributing the nodes after each parameter continuation step was (cf. Thompson, Warsi & Mastin 1985)

$$W(x) = (1 + \gamma^2|k|)(1 + \alpha^2 p_x^2)^{1/2},$$

where p_x is the slope and $k \equiv p_{xx}/(1 + p_x^2)^{3/2}$ is the curvature of the pressure profile. Close spacing of nodes where the gradient is high is emphasized by making α large, whereas concentration where curvature is high is emphasized by making γ large. Choosing $\alpha = 1$ and $\gamma = 1$ seemed to make computing time (CPU time) minimum or nearly so.

Between successive Newton iterations at a given parameter set, the fraction of the total domain length occupied by each interval remained constant as the outflow boundary node moved in order to satisfy the film-split condition, (9).

3. Cross-flow instabilities: onset of ribbing

If the roll surface speed is too fast, or the liquid viscosity too high, the film-split meniscus in forward roll coating becomes wavy in the cross-flow direction and the films emanating from it become ribbed (see figure 2). In this section, a stability analysis of forward deformable roll coating is developed for positive gaps and the linear spring model of roll cover deformation. The goal is to predict the critical parameters at which the onset of ribbing occurs and to study how the roll deformation may affect this flow instability.

3.1. *Formulation of the linear stability analysis*

It is assumed that the wavy character can be attributed to a small perturbation in the uniform film-split meniscus that grows with time. Thus the first step in the linear stability analysis is to perturb the steady-state flow with an infinitesimal sinusoidal disturbance in the transverse direction, as illustrated in figure 7:

$$\left.\begin{aligned} x_m^*(z,t) &= x_m + \epsilon e^{\beta t}\sin(2\pi n z),\\ p^*(x,z,t) &= p(x) + g(x)\epsilon e^{\beta t}\sin(2\pi n z),\\ h^*(x,z,t) &= h(x) + Ne\ g(x)\epsilon e^{\beta t}\sin(2\pi n z). \end{aligned}\right\} \tag{12}$$

Here the small parameter ϵ is the amplitude of the transverse disturbance, n is its wavenumber ($\lambda \equiv 1/n$ is the wavelength), and β is its growth factor. The growth factor is a function of the wavelength. On the grounds that in reality disturbances of all wavelengths are present, arising from molecular fluctuations if not external influences, the wavelength for which β is largest is taken to be the most dangerous, i.e. the fastest growing and likely to be close to the wavelength of the finite-amplitude

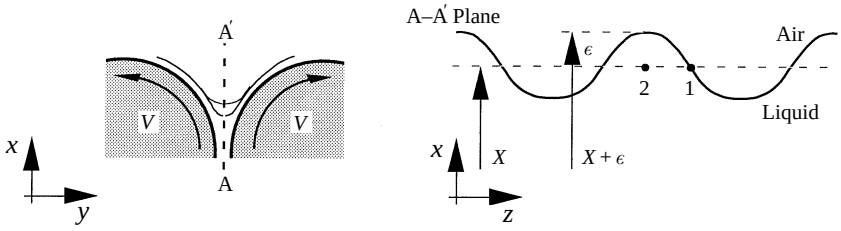

FIGURE 7. The film-split meniscus is perturbed in the transverse direction z by a sinusoidal disturbance.

ribbing that develops if β is positive. If β is negative at all wavelengths, all infinitesimal disturbances decay in time and the system is said to be stable.

The unperturbed variables x_m, $p(x)$ and $h(x)$ describe the base flow, i.e. they are the solution of the steady-state one-dimensional problem, given by equations (11).

The disturbed variables must satisfy the time-dependent two-dimensional Reynolds equation:

$$\frac{\partial}{\partial x}\left(h^{*3}\frac{\partial p^*}{\partial x}\right)+\frac{\partial}{\partial z}\left(h^{*3}\frac{\partial p^*}{\partial z}\right)=12\left(\frac{\partial h^*}{\partial x}+\frac{\partial h^*}{\partial t}\right).$$

Replacing the perturbed variables, (12), and dropping the terms of order ϵ^2 and higher leads to an ordinary differential equation that governs the amplitude function $g(x)$:

$$\frac{\mathrm{d}^2 g}{\mathrm{d}x^2}+\left\{\frac{3\ Ne}{h(x)}\frac{\mathrm{d}p}{\mathrm{d}x}-\frac{12\ Ne}{h(x)^3}+\frac{3}{h(x)}\frac{\mathrm{d}h}{\mathrm{d}x}\right\}\frac{\mathrm{d}g}{\mathrm{d}x}$$
$$+\left\{\frac{6\ Ne}{h(x)^2}\frac{\mathrm{d}p}{\mathrm{d}x}\frac{\mathrm{d}h}{\mathrm{d}x}+\frac{3\ Ne}{h(x)}\frac{\mathrm{d}^2 p}{\mathrm{d}x^2}-4\pi^2 n^2-\frac{12\beta Ne}{h(x)^3}\right\}g=0, \tag{13}$$

Because the disturbances of interest are those that distort the free surface, the pressure far upstream is presumed to be unperturbed, which implies that

$$g(-\infty)=0. \tag{14}$$

In the same way, placing the perturbed variables (12) in the pressure boundary condition at the film-split meniscus (11c) and dropping terms of order ϵ^2 and higher leads to a boundary condition on $g(x)$ at the film-split meniscus:

$$g(x_m)=\frac{-\left(\dfrac{\mathrm{d}p}{\mathrm{d}x}\right)_{x_m}+\dfrac{1}{Car_m h(x_m)}\left(\dfrac{H_0}{R}\right)^{1/2}\left(\dfrac{\mathrm{d}h}{\mathrm{d}x}\right)_{x_m}+\dfrac{4\pi^2 n^2}{Ca}\dfrac{H_0}{R}}{1-\dfrac{Ne}{Car_m h(x_m)}\left(\dfrac{H_0}{R}\right)^{1/2}}. \tag{15}$$

The growth factor β is evaluated by imposing continuity of flow toward and away from the film-split meniscus:

$$\beta=\frac{1}{F(1+S^{2/3})-1}\frac{h^2(x_m)}{12}\left\{\left(\frac{\mathrm{d}g}{\mathrm{d}x}\right)_{x_m}+\left(\frac{\mathrm{d}^2 p}{\mathrm{d}x^2}\right)_{x_m}\right.$$
$$\left.+\frac{2}{h(x_m)}\left(\frac{\mathrm{d}p}{\mathrm{d}x}\right)_{x_m}\left[\left(\frac{\mathrm{d}h}{\mathrm{d}x}\right)_{x_m}+Ne\ g(x_m)\right]\right\}, \tag{16}$$

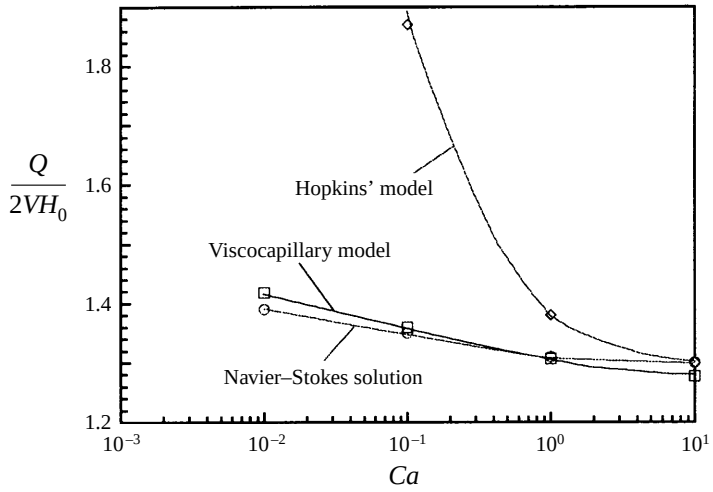

FIGURE 8. Comparison of the flow rate predictions of Hopkins' model, viscocapillary model and Navier–Stokes solution. $H_0/R = 10^{-2}$.

where

$$F \equiv \frac{h_B}{h(x_m)}.$$

The equation system governing the amplitude function $g(x)$ consists of the second-order differential equation (13) and boundary conditions (14) and (15). The growth factor β, given by (16), appears in one of the coefficients of (13). The nodes used to discretize the differential equation are the same ones used to integrate Reynolds' equation for the base flow.

A simple Picard iteration was used to solve this nonlinear system. Generally, convergence was obtained in 3 or 4 iterations. For a given base flow, the growth factor β was calculated at 200 different wavenumbers n, and the CPU time consumed for this task was around 2 s in a HP workstation, series 735.

4. Results

Although the mathematical formulation presented in the previous section is valid at any speed ratio other than zero, the results presented here are restricted to the symmetric case, i.e. $S = 1$.

4.1. *Comparison of models of flow in gaps between rigid rolls*

Before examining analyses of flow in deformable gaps, it is instructive to compare the viscocapillary model of flow between rigid rolls with earlier models, in which Hopkins' boundary condition was used at the film split, and with solutions of the Navier–Stokes system at vanishing Reynolds and Stokes number (Coyle *et al.* 1986). In figure 8 dimensionless flow rate q in symmetric film-split flow is plotted versus dimensionless average roll speed, or capillary number; in figure 9, film-split location downstream of the minimum clearance is plotted.

At small capillary number ($Ca < 1$), the effect of surface tension acting through capillary pressure at the film-split meniscus is strong enough that the viscocapillary model predicts flow rates within 5% of the Navier–Stokes solution, and the film-split

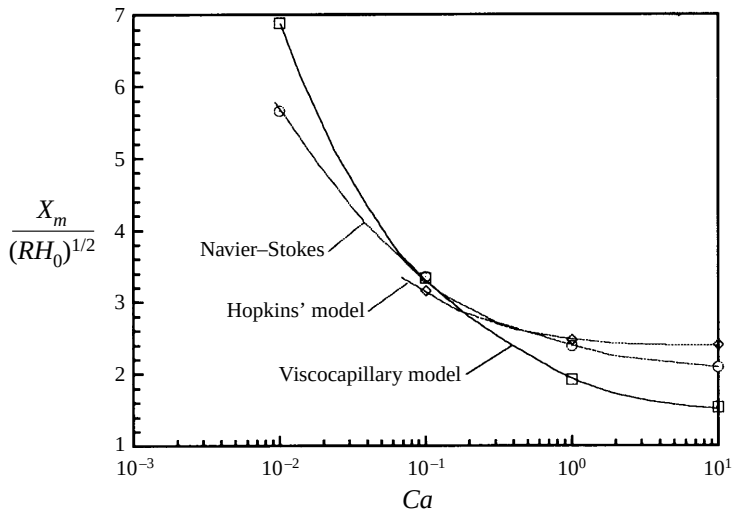

FIGURE 9. Comparison of the position of meniscus predictions of Hopkins' model, viscocapillary model and Navier–Stokes solution. $H_0/R = 10^{-2}$.

location within 15%. Although the meniscus position predicted by Hopkins' model is close to the complete two-dimensional solution, the flow rate is largely overpredicted (see figure 8).

Surprisingly, the predictions of the viscocapillary model at capillary number of the order of 1 are still close to the Navier–Stokes solution, even though the Landau–Levich equation is not valid at $Ca = 1$. At this value of capillary number, the results obtained with the Hopkins' boundary condition still overpredicts the flow rate through the gap.

At capillary number of the order of 10, which is less often encountered in roll coating practice, the effects of viscous stress are strong enough that Hopkins' boundary condition leads to predictions closer to the Navier–Stokes solution.

The largest capillary number explored in this work is of the order of 1. Because the viscocapillary predictions obtained at this value are still close to the Navier–Stokes solution, we used the viscocapillary model for all sets of parameters.

4.2. *One-dimensional base flows*

In the spring model of roll cover deformation, the elasticity number $Es \equiv \mu\overline{V}/KR^2$ appears only in combination with the ratio of roll radius to half-gap, R/H_0 (or diameter to gap), in what is called the modified elasticity number *Ne*. Thus, a change in *Ne* can be ascribed variously to changes in the centre-to-centre distance, as reflected in H_0, or the spring constant K, which would represent a change in the elastic modulus E, cover thickness L, or Poisson's ratio v. For clarity, however, the predictions of the model are presented in terms of the ordinary elasticity number $Es \equiv \mu\overline{V}/KR^2$, the capillary number $Ca = \mu\overline{V}/\sigma$, and the dimensionless gap H_0/R. In flow through deformable (positive) gaps, typical values of these dimensionless parameters are

$$\frac{\mu\overline{V}}{KR^2} \approx 0 \text{ to } 10^{-6}, \quad \frac{H_0}{R} \approx 10^{-4} \text{ to } 10^{-2}, \quad Ca = \frac{\mu\overline{V}}{\sigma} \approx 10^{-3} \text{ to } 1.$$

Figure 10 shows that when the gap is large enough, the pressure which develops between the rolls is insufficient to deform appreciably the rubber cover and the flow

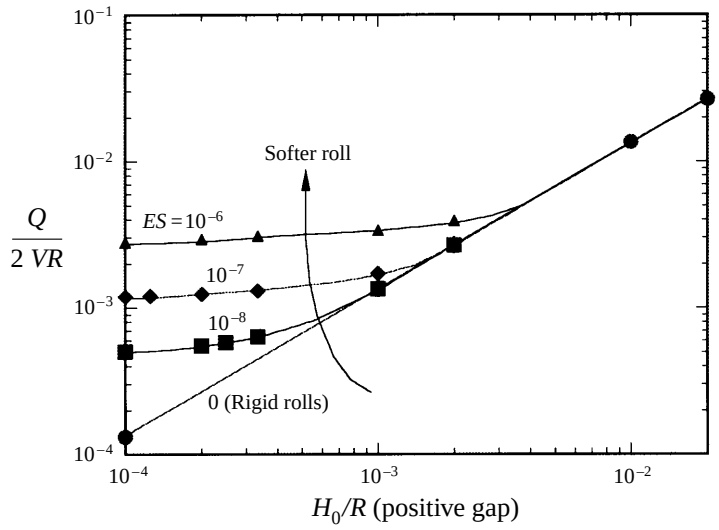

FIGURE 10. Flow rate at different undeformed gaps and elasticity numbers. $Ca = 0.1$.

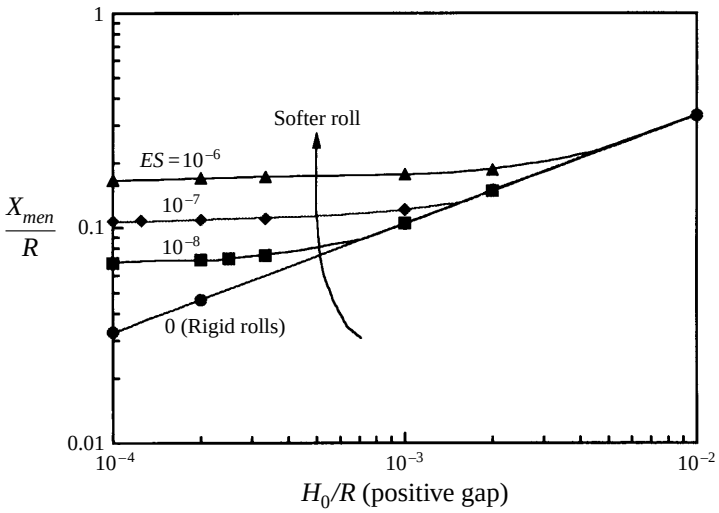

FIGURE 11. Film-split location at different undeformed gaps and elasticity numbers. $Ca = 0.1$.

rate is linear with clearance, just as with two rigid rolls. As the gap is narrowed and higher pressure develops, the rubber cover deforms and the flow rate is greater than between rigid rolls at the same (undeformed) gap. More importantly, the effect of the (undeformed) gap setting diminishes as the gap is narrowed and the roll cover made softer – regardless of capillary number, whose effect is small and not shown. This lessened sensitivity to gap and roll cover is one of the advantages of using a rubber-covered roll.

Figure 11 shows that when the gap is large enough the film split location approaches the rigid rolls configuration, but as the gap is narrowed the deformation of the roll forms a more and more elongated channel of very nearly constant clearance, as depicted in figure 12, and the film split locates further and further upstream – all at a fixed capillary number. Figure 13 shows that as capillary number falls, for instance by

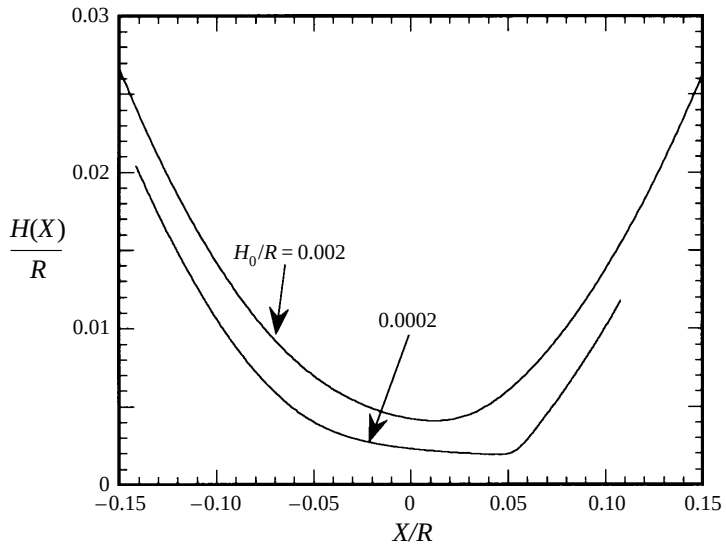

FIGURE 12. Roll profiles at different undeformed gaps. $Es = 10^{-7}$, $Ca = 0.1$.

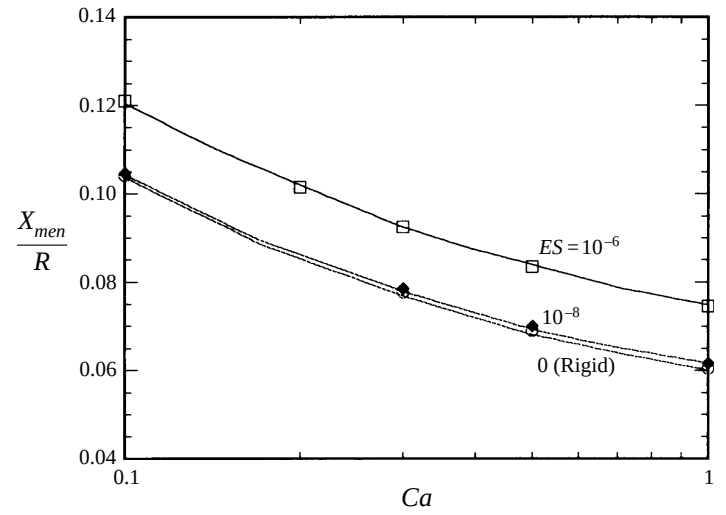

FIGURE 13. Film-split location versus capillary number. $H_0/R = 10^{-3}$.

raising surface tension, and as the elasticity number increases, for instance by making the roll softer, the film split is drawn downstream.

The pressure peak in the converging part of the gap and its valley in the diverging part become more pronounced as the rolls are moved closer together, as in plain from figure 14. There the profiles terminate at the film split, where the subambient pressure is due to the capillary pressure jump at the curved interface or meniscus. The jump is greater the narrower the undeformed gap because the meniscus is more sharply curved. The narrower the gap, the longer the region of nearly constant (negative) pressure gradient, which coincides with the region of nearly constant clearance: the flow there is a virtually constant combination of drag flow and pressure-gradient-driven flow. The bottom of the pressure valley is the lowest pressure in the flow. If it is below the

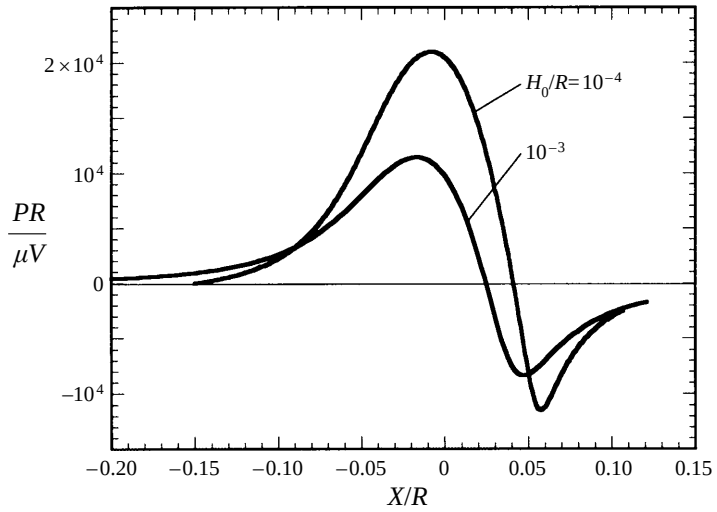

FIGURE 14. Pressure distribution at different centre-to-centre distance, i.e. undeformed gaps. $Es = 10^{-7}$, $Ca = 0.1$.

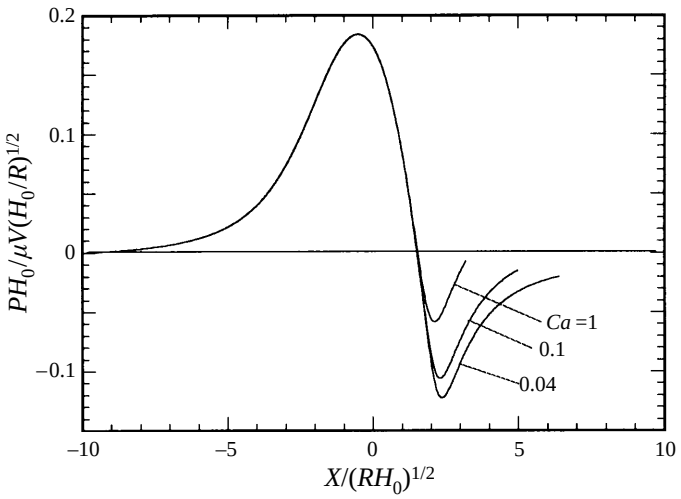

FIGURE 15. Pressure distribution at different capillary numbers. $Es = 10^{-8}$, $H_0/R = 2 \times 10^{-4}$.

sum of the partial pressure of dissolved gas and the vapour pressure of the liquid, a potential exists for cavitation in the flow: all that needed are nuclei of bubble growth.

Figure 15 shows that as the effect of surface tension rises and capillary number falls, not only does the film split locate further downstream and its meniscus curvature diminish, but also the pressure gradient lessens. Because the instability that leads to a wavy free surface in the transverse direction is driven by this pressure gradient (cf. Pearson 1960), the likelihood of ribbing falls with capillary number, just as between rigid rolls.

The effect of elasticity number on the pressure profile, at fixed capillary number and roll spacing, i.e. undeformed gap, is illustrated in figure 16. The higher the elasticity number, i.e. the softer the roll, the more the resilient cover deforms and the wider the channel it makes with the hard roll. This change in gap conformation lessens the

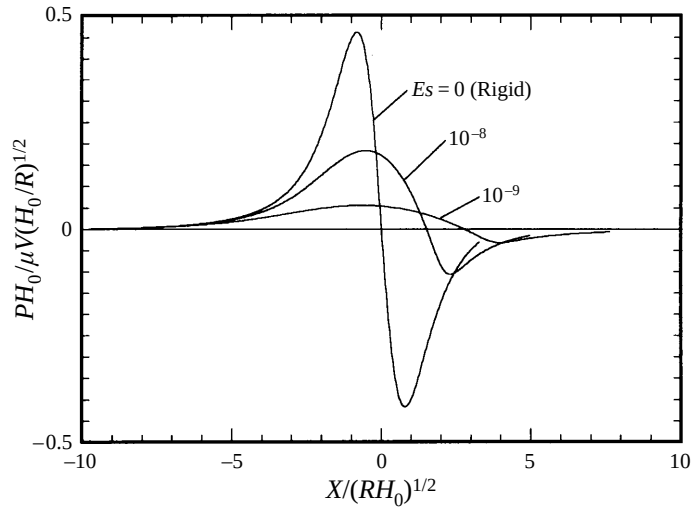

FIGURE 16. Pressure distribution at different elasticity numbers. $H_0/R = 2 \times 10^{-4}$, $Ca = 0.1$.

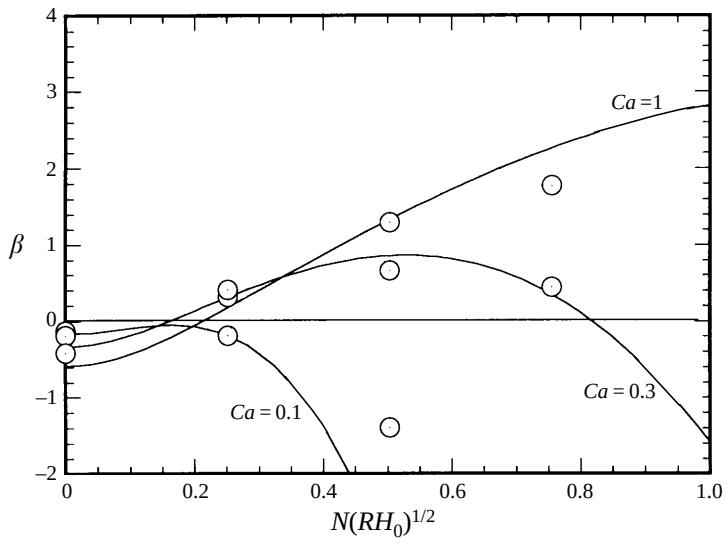

FIGURE 17. Growth factor β as function of wavenumber at different capillary numbers. Case of rigid roll and $H_0/R = 10^{-3}$. Curves are predictions of the viscocapillary model and circles are Navier–Stokes solutions.

maximum and minimum pressure, elongates the region of nearly constant gap (the 'footprint' of the deformable roll), and moderates the pressure gradient just upstream of the film meniscus. This last is related to the critical capillary number for the onset of ribbing. That the deformation of the roll cover can delay the onset of ribbing is confirmed by the stability analysis that follows.

4.3. *Theoretical predictions of ribbing onset and pattern*

The stability of each steady state was found by solving (13)–(16) and examining the growth factor β, in units of $\overline{V}/(RH_0)^{1/2}$, versus disturbance wavenumber n, in units of $1/(RH_0)^{1/2}$: see figure 17. This figure shows that when both rolls are rigid,

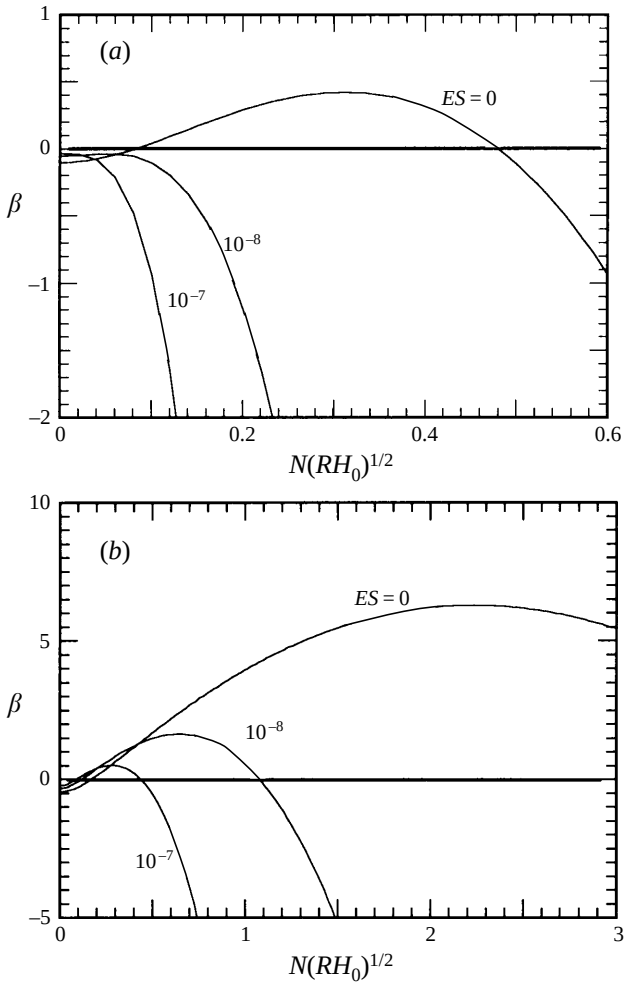

FIGURE 18. Growth factor versus wavenumber at different elasticity numbers and capillary numbers equal to (*a*) 0.05 and (*b*) 0.5. $H_0/R = 10^{-4}$.

the steady flow is stable at values of the capillary number up to about 0.1, and is unstable at higher values. Moreover, as the capillary number rises, the fastest-growing disturbance (whose wavelength is at the maxima in the plotted curves) shifts to progressively higher wavenumbers. As capillary number rises, the wavenumber of the most dangerous perturbation increases and thus the wavelength of the perturbed meniscus decreases. In figure 17 the open circles are more accurate predictions computed at $Re = 0$ and $St = 0$ from the full Navier–Stokes theory by Coyle, Macosko & Scriven (1990). Despite the approximations in the viscocapillary model, its predictions agree with those of Navier–Stokes theory, except at the higher wavenumbers at $Ca = 0.1$ and 1. The computational cost of the viscocapillary model is much smaller than for the solution of the full Navier–Stokes system and the eigenvalue problem that arises from the linear stability analysis described by Coyle *et al.* (1990).

The growth factor as function of wavenumber at capillary numbers of 0.05 and 0.5 and at different elasticity numbers is shown in figure 18. When the rolls are rigid, i.e.

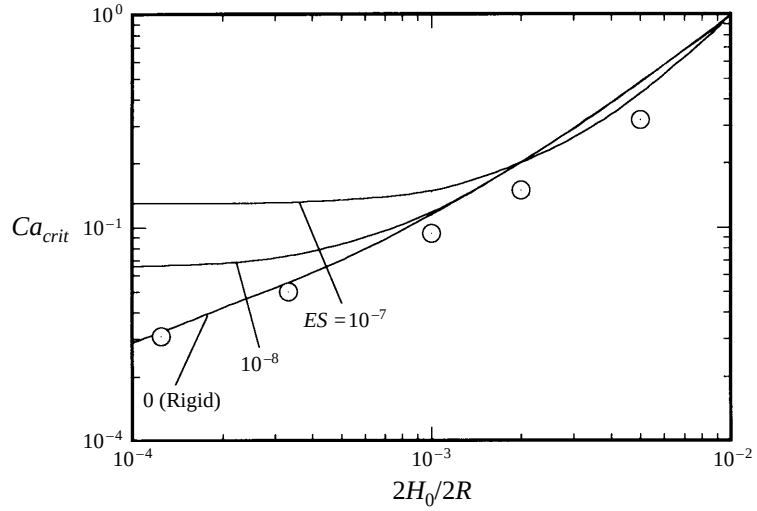

FIGURE 19. Critical capillary number for the onset of ribbing as function of undeformed gaps and elasticity numbers. Curves correspond to viscocapillary model predictions and circles to Navier–Stokes solutions.

when the elasticity number is zero, the flow is unstable at both capillary numbers. The flow is stable, i.e. the coated film remains uniform in the transverse direction, at elasticity number larger than 10^{-8} when the capillary number is 0.05. Thus, the deformation of the roll cover delays the onset of ribbing.

The critical capillary number is the value at which the growth rate vanishes, i.e. at the onset of instability, or marginal stability. It is plotted versus roll separation in figure 19. The curve for rigid rolls accords with Coyle *et al.*'s (1990) results – the open data points – though not as well at greater roll separations (larger ratios of undeformed gap to roll diameter) as at smaller ones. The previous lubrication-based stability analysis (Savage 1984 and Fall 1985) underpredicted the critical capillary number by as much as 90%. At this range of capillary number, the boundary condition used here, i.e. the Landau–Levich film flow equation, gives a much better description of the flow near the film-split meniscus. As a soft and a hard roll are pushed together, the onset of ribbing is delayed to higher capillary numbers, or to higher coating speeds when viscosity and surface tension are fixed. The softer the roll, i.e. the larger the elasticity number, the higher the critical capillary number at a given roll separation. This is one of the advantages of using deformable gaps in forward roll coating.

The roll cover deformation also alters the wavelength of the ribbing pattern. At a capillary number of 0.5, the flow is unstable at all three elasticity numbers shown in figure 18(*b*), but the most dangerous wavenumbers differ significantly. At fixed roll separation and capillary number, the softer the roll, i.e. the larger the elasticity number, the smaller is the wavenumber, i.e. the larger the ribbing wavelength. The larger the wavelength of the fastest growing disturbances, the slower the rate of levelling (cf. Anshus 1973). So, there are trade-offs to be made in choosing roll covers.

At any given roll separation, beyond the roll speed at which ribbing becomes visible, the wavelength falls as speed is raised (figure 20). Because the rate of levelling of ribbing is proportional to an inverse power of wavelength as high as the fourth when

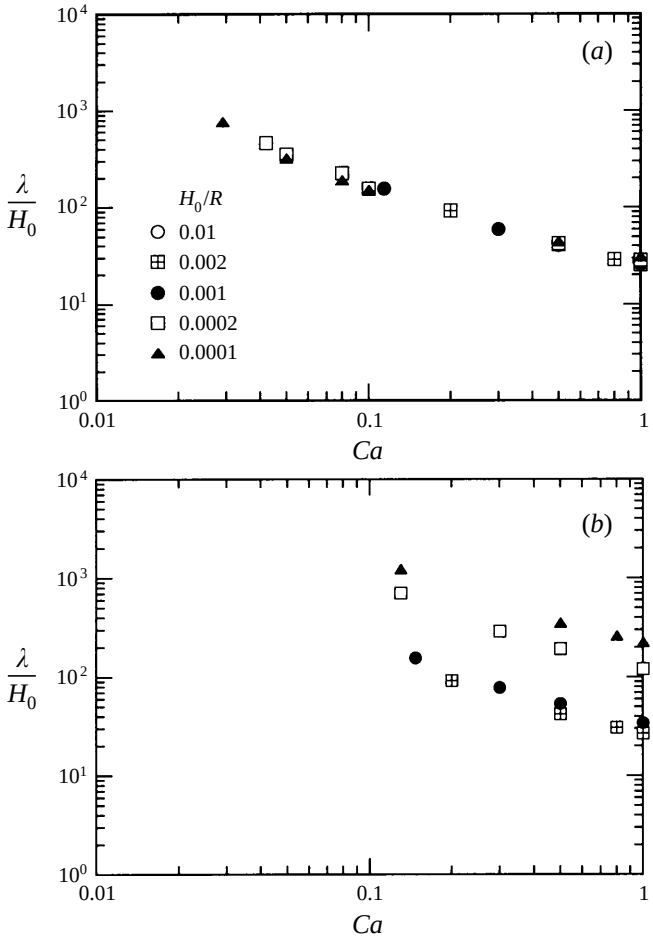

FIGURE 20. Wavelength as function of capillary number at elasticity number equal to (*a*) 0 (Rigid rolls) and (*b*) 10^{-7}.

the liquid is Newtonian (Orchard 1962 and Anshus 1973), the effect on ultimate film uniformity can be profound and paradoxical, if the ultimate smoothness is enhanced by raising roll speed.

An interesting feature is that, for rigid rolls, the predictions of wavelength, in units of half-gaps, at different rolls separation all lie in a band that could be approximated by a single curve. At an elasticity number of 10^{-7} and $H_0/R > 10^{-3}$ the resilient cover does not deform appreciably and the results match those from rigid gaps. At small enough gaps, i.e. $H_0/R < 2\times10^{-4}$, the dimensionless wavelength λ/H_0 generated from a deformable gap is larger than those generated from rigid gaps.

The foregoing comparisons of the performances of deformable gaps and rigid ones are all at fixed capillary number and roll separation, or undeformed gap. At a fixed capillary number and gap, the flow rate through a deformable gap is greater than through a rigid one because the resilient cover is compressed by the pressure that develops in the flowing liquid. For practical purposes, it is better to compare the performances at a given layer thickness on one of the rolls, for that is what is often specified by the product design. It is appropriate to compare gap performances on

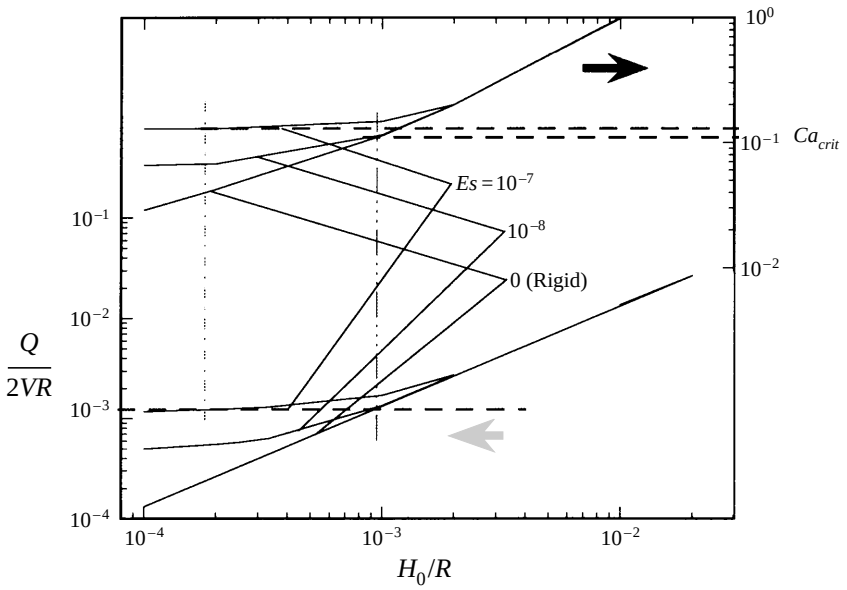

FIGURE 21. Comparison of critical capillary number for onset of ribbing at a fixed layer thickness and at different elasticity numbers.

the basis of fixed flow rate but different roll separations. To do so requires combining information on how the flow rate, undeformed gap and elasticity number (roll cover elastic modulus) are interrelated, and on the critical capillary number for the onset of ribbing in each situation.

Figure 21 combines figures 10 and 19. The flow rate in units of roll diameter, i.e. $Q/2VR$, varies little with capillary number and can be taken as independent of it. For different roll covers (elasticity numbers) the gap-to-diameter ratio to obtain a given layer thickness $h^*/2R = Q/2VR$ can be read from the lower part of figure 21 and the critical capillary numbers at the onset of ribbing can be read from the upper part. The critical capillary number is higher the softer the roll. Therefore, for a given coated layer thickness, or coat weight, the softer the roll, the higher the operating speed that still yields a satisfactorily smooth coating, according to the viscocapillary model.

5. Experimental study

In order to verify the predictions of the viscocapillary model, experiments were conducted to obtain the critical capillary number above which ribbing occurs for both rigid and deformable gaps. A relative simple new detection technique was used to find the critical conditions at apparent onset of ribbing and, for the first time, at the onset of unsteady, or wandering ribbing.

5.1. *Experimental set-up*

The experimental set-up is sketched in figure 22. The left roll, which can be either rigid or soft, is in a stationary mounting; the right roll can be adjusted horizontally to change the gap. The gap was determined with two micrometers, one attached to each side of the adjustable mounting.

The critical capillary number for onset of ribbing and the ensuing ribbing pattern depend on the clearance between the roll surfaces (Pearson 1960). So, to obtain a

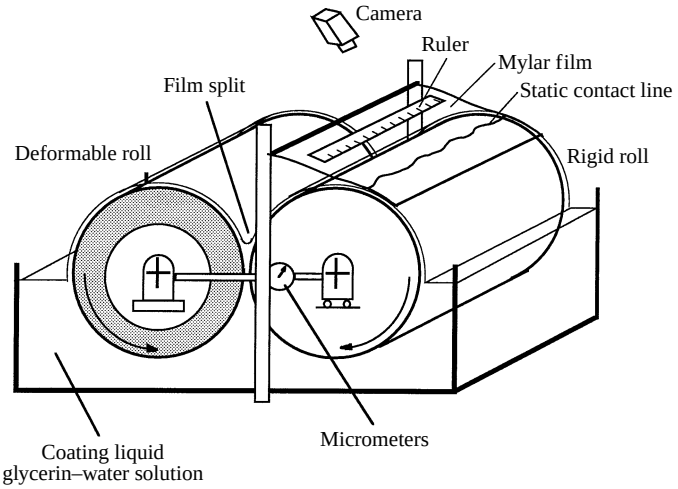

FIGURE 22. Sketch of experimental set-up.

perfectly uniform ribbing pattern in the cross-web direction, the rolls have to be perfectly parallel to each other. In this work, the degree of uniformity of the ribbing wavelength in the transverse direction was used as an indicator of how nearly parallel the rolls were.

The rolls were 20.3 cm in diameter and approximately 30.5 cm in length. The soft roll was covered with a 13 mm thick rubber cover with a hardness of 40 durometer, which would correspond to an elastic modulus of about 1.4×10^6 Pa, were the rubber ideal (Payne & Scott 1960). The runout of the surface of the rigid roll in its bearings was 25 μm; of the soft roll, 10 μm.

The liquid used in the experiments was a glycerin–water solution of about 70% weight glycerin. The viscosity varied from 92 to 115 cP and the surface tension was about 56 mN m^{-1} at room temperature, i.e. 22 to 23°C.

The capillary numbers at the onset of ribbing in symmetric film-splitting between rigid rolls reported by Pitts & Greiller (1961), Mill & South (1967), Greener *et al.* (1980) and Benkreira, Edwards & Wilkinson (1982) show the same trends and fall in a narrow range, but vary by as much as 200% at some gap-to-diameter ratios. The reason is the subjective nature of 'ribbing onset', as documented by Coyle *et al.* (1990). In the present work too, it was found that as the rolls were sped up (viscosity and surface tension fixed), the transition from a smooth to a wavy meniscus in the film split was gradual, and that detecting the transition depended on the way in which the scene was illuminated, magnified and viewed. Because our objective was to compare performances of deformable and rigid gaps, the criterion used was not critical, provided it was the same in both cases. The criterion we chose is described in the following paragraph.

To measure wavelength easily we chose to observe the static contact line where the surface of the liquid layer on one of the rolls intersected a flexible transparent sheet of polyethylene terephthallate (PET) mounted as though to smooth the layer, as shown in figure 22. The PET sheet was 120 μm thick, 200 mm long, and fastened to a horizontal bar located about 90° circumferentially downstream of the film split. The arrangement was such that the sheet removed no liquid from the roll surface and did leave the layer totally smooth to the eye, except at speeds high enough (around 1 m s^{-1}) that air fingering could be observed through the PET. The image of the

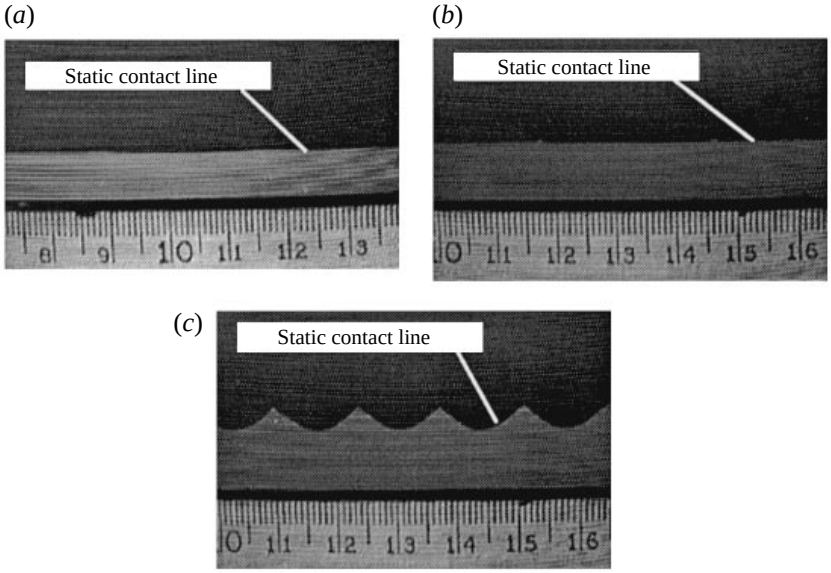

FIGURE 23. Static contact line at Mylar film at a gap = 250 μm: (*a*) roll speed = 0.13 m s^{-1}; (*b*) roll speed = 0.15 m s^{-1} and (*c*) roll speed = 0.24 m s^{-1}.

static contact line was viewed through the transparent sheet and was recorded with a camera placed above it.

If the liquid layer arriving at the PET film was uniform in the transverse direction, the static contact line was straight. The onset of ribbing was taken to be the first visually detectable (unmagnified), apparent periodic (*not* sinusoidal) distortion of the straight line, as shown in figure 23(*a*) (gap of 250 μm and speed of 0.13 m s^{-1}). What was detectable under the conditions adopted, we estimated to be about 4 μm displacement over a length of 7 cm. As the speed was increased, the ribbing became more apparent, as illustrated in figure 23(*b*) (gap of 250 μm and speed of 0.15 m s^{-1}) and figure 23(*c*) (gap of 250 μm and speed of 0.24 m s^{-1}). The wavelength λ_0 of the distortion corresponded the wavelength λ of the ribbing, however the pattern observed in the PET sheet did not correspond to a cross-section of the film profile.

The undeformed gaps were varied from 50 to 750 μm (in one case the gap was nominally 20 μm), the recorded value being the average of measurements across the roll width.

At each gap setting the speed of the rolls was raised in increments of 1 r.p.m. until the static contact line displayed a perceptible distortion that was approximately periodic along its length. This speed was taken to be the critical capillary number. Raising the roll speed was then resumed and amplitude as well as wavelength were measured. At a higher speed a second transition was encountered: the ribbing ceased to be steady, instead migrating back and forth in the transverse direction, individual ribs merging and dividing. The second transition we call the onset of unsteady ribbing. Though the phenomenon must be common, it has not been reported in previous roll coating studies, as far as we know. A similar phenomenon recently caught the attention of physicists studying a flow in the annular space between two cylinders (Rabaud, Michalland & Couder 1990).

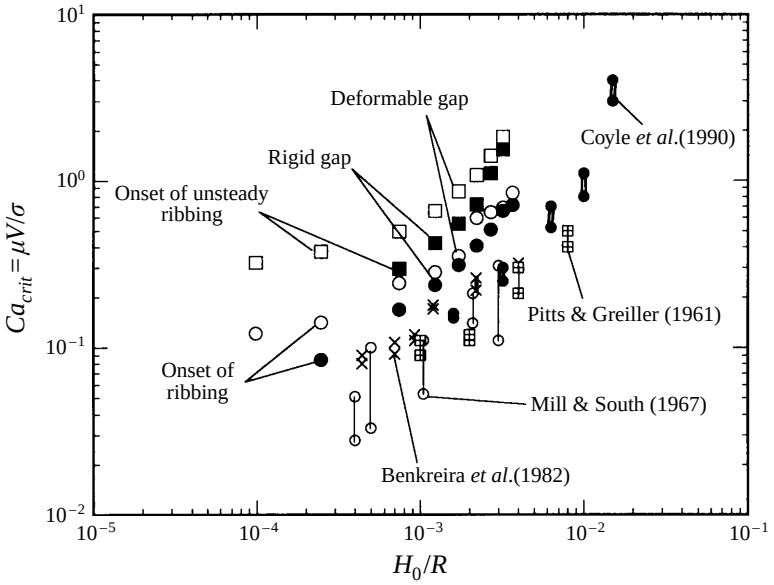

FIGURE 24. Critical capillary number for the onset of ribbing at rigid and deformable gaps.

5.2. *Results and discussion*

In figure 24 the critical capillary numbers at the onset of ribbing in both rigid and deformable gaps are compared with values from rigid gaps reported by other researchers.

The onset of (steady) ribbing obtained with the Mylar film technique is at capillary numbers 50 to 100% higher than the power-law correlation adopted by Mill & South, 120% higher than the correlation of Pitts & Greiller's experimental observations, and 20 to 90% higher than the critical capillary numbers reported by Benkreira *et al.* But the trend with gap is the same. Coyle *et al.* (1990) explained that ribbing amplitude rises abruptly around the capillary number that would be critical if the smooth flow were truly two-dimensional. Thus it appears that the detection technique we chose in this work is somewhat less sensitive than the illumination and viewing set-ups employed by past investigators. One reason for this is that here the onset of apparently periodic distortion of the coated film was being observed 90° downstream from the film-split meniscus. All past researchers were looking directly at the film-split meniscus or reflected images of it. Nevertheless our technique is adequately accurate for our purpose of comparing the performances of rigid and deformable gaps and gives accurate measurements of the wavelength of ribbing patterns.

The critical roll velocity (capillary number) is a function of the minimum clearance between the rolls. At small gaps (50 μm) the maximum velocity at which visually uniform film could still be obtained was 0.05 m s^{-1}. As the gap widens, the critical velocity (capillary number) increases; it is 0.4 m s^{-1} at a gap of 750 μm. A uniform film can be obtained at a much faster speed.

When the gap is relatively wide compared to the roll diameter, i.e. when the ratio of half-gap to roll radius is large enough, e.g. $H_0/R > 2 \times 10^{-3}$ (refer to figure 24), the capillary numbers at ribbing onset in the deformable gap and in the rigid gap are the same. In wide gaps, the pressure that develops in the liquid is not enough to deform the resilient cover. In narrower gaps, however, ribbing first appears downstream of a

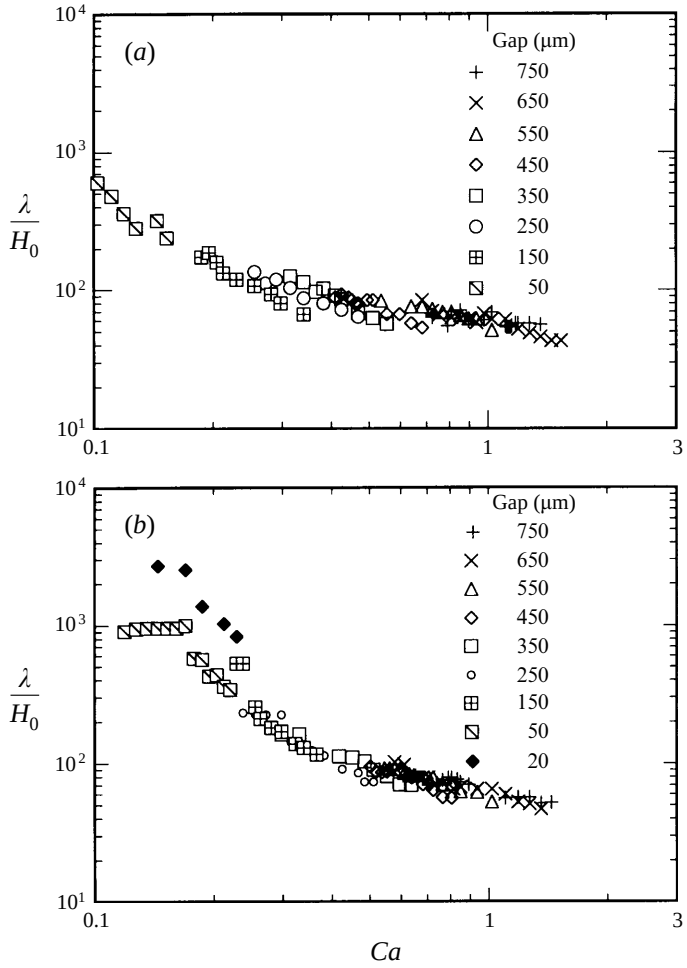

FIGURE 25. Wavelength, in units of half-gap, of ribbing from (*a*) rigid and (*b*) deformable gaps.

deformable gap at capillary numbers higher than in a rigid gap. Thus an apparently smooth liquid layer can be obtained from the forward-roll film split at a deformable gap at a higher speed than from a rigid gap. The speed advantage is only 5% in a relatively wide gap ($H_0/R \approx 1\times10^{-3}$) but climbs to 60% in a narrower gap ($H_0/R = 2.5\times 10^{-4}$). The delay in the onset of ribbing when a deformable roll is used accords qualitatively with the theoretical predictions of the viscocapillary model (see figure 19).

Figure 25*a* shows ribbing wavelength λ in units of half-gap H_0, i.e. the ratio λ/H_0, versus capillary number $\mu\overline{V}/\sigma$ from rigid gaps of 50 to 750 μm. At any given gap, after the roll speed is great enough that ribbing is visible, the wavelength falls as speed is raised. This behaviour is illustrated by the photographs in figure 26. The wavelength was divided by almost three as the roll speed was increased from 0.15 m s^{-1} to 0.24 m s^{-1}. The viscocapillary model presented here was able to predict well this tendency – see figure 20(*a*). The experimental data from the different gaps also lie in a band (figure 25*a*), as predicted by the viscocapillary model.

Figure 25*b* shows ribbing wavelength versus capillary number measured in deformable gaps of nominal clearance from 20 to 750 μm. At large roll separation

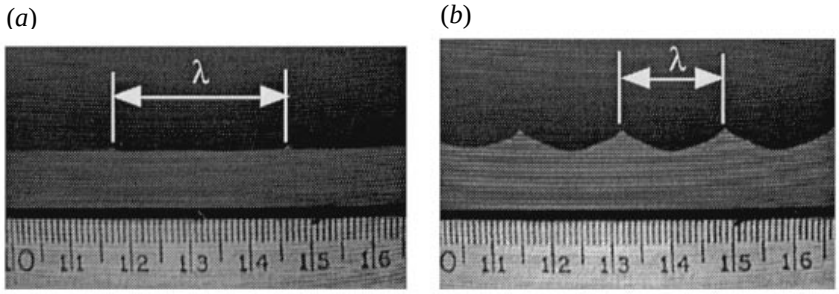

FIGURE 26. Static contact line at gap = 250 μm and (*a*) roll speed = 0.15 m s^{-1}; and (*b*) roll speed = 0.24 m s^{-1}.

the resilient roll cover does not deform appreciably and the results reproduce those from the rigid gaps. At small roll separation there is a major difference: at the same capillary number the wavelength generated by the deformable gaps is greater than that generated by the rigid gaps. The ratio is 2 at a gap of 250 μm and capillary number of 0.3 and appears to be as high as 5 at a gap of 50 μm and capillary number of 0.15. Consequently the rate of levelling of ribbing downstream of the film split may be substantially slower when a deformable gap is used. The viscocapillary model presented here was able to predict well this behaviour – see figure 20(*b*).

6. Conclusion

Flow between deformable rotating rolls was analysed using lubrication theory, coupled with a one-dimensional elastic model of the resilient roll cover and the film-flow equation to describe the film-split region. With this new boundary condition for Reynolds' equation at the free-surface meniscus, the results yielded by lubrication theory were in accordance with the complete Navier–Stokes solution, even at low capillary numbers.

The stability of the base lubrication flow to transverse disturbances was analysed by examining the time-dependent two-dimensional response to infinitesimal perturbations in order to identify those that grow fastest. The critical capillary numbers for the onset of ribbing obtained with the analysis presented here were in close agreement with linear stability analysis applied to the solutions of the two-dimensional Navier–Stokes system. Previous results using the lubrication approximation underpredicted the onset of ribbing.

The results presented show how different parameters can affect the performance of a deformable roll gap, and can be used to infer how a deformable cover can be used to optimize the process, i.e. obtain a smooth film at higher line speeds.

Experiments were performed in order to validate the predictions. The critical capillary numbers for the onset of ribbing in rigid gaps were higher than previously reported in the literature. The reason is that we were observing the coated film 90° downstream the film-split meniscus and some levelling may have occurred. However, the technique adopted in this work gives accurate measurements of the wavelength of the ribbing pattern and is adequate for comparing the performance of rigid and deformable gaps.

The behaviour observed in the experiments shows the same trends as the visco-capillary model predictions: the onset of ribbing occurred at higher capillary number

when a deformable gap was used and the ribbing wavelength falls as capillary number rises.

This analysis can be extended to the case where the undeformed roll surfaces would interfere, i.e. a negative gap. Viscoelastic effects of the rubber cover can be introduced in the formulation by using a combination of springs and dashpots in place of the linear springs used here (cf. Carvalho & Scriven 1994*b*).

The viscocapillary model predicts an even film split if the rolls have the same speed, i.e. speed ratio equal to unity. Experimental evidence shows that this is not always true. Details on the effect of roll deformation on the film split can be found by solving the complete Navier–Stokes equation coupled with plane-strain deformation for resilient roll cover.

T. J. Anderson provided skilled assistance with the experimental study. M. S. Carvalho was supported by a fellowship from CAPES (Department of Education, Federal Government of Brazil). Further support came from cooperating corporations through the Center for Interfacial Engineering and was supplemented by the National Science Foundation and from computational grants from the Minnesota Supercomputer Institute.

REFERENCES

Anshus, B. E. 1973 The leveling process in a polymer powder painting – a three-dimensional approach. *Am. Chem. Soc. Div. Org. Coating Plastic Chem.* **33.2**, 493.

Benkreira, H., Edwards, M. F. & Wilkinson, W. L. 1982 Ribbing instability in the roll coating of Newtonian fluids. *Plastics Rubber Processing Applic.* **2**, 137.

Benjamin, D. F., Anderson, T. D. & Scriven, L. E. 1995 Multiple roll systems: steady state operation. *AIChE J.* **41**, 1045.

Benner, R. E., Davis, H. T. & Scriven, L. E. 1987 An adaptive finite element method for steady and transient problems. *SIAM J. Sci. Statist. Comput.* **8**, 529.

Cameron, A. 1966 *Basic Lubrication Theory*. Wiley.

Carvalho, M. S. & Scriven, L. E. 1994*a* Effect of deformable roll cover on roll coating. *TAPPI J.* **77**, 201.

Carvalho, M. S. & Scriven, L. E. 1994*b* Capillary and viscoelastic effects on elastohydrodynamic lubrication flow and film-splitting in roller nips. *Proc. 1994 Intl Printing and Graphics Arts Conference, Hallifax, Canada.* TAPPI Press.

Coyle, D. J. 1988 Forward roll coating with deformable rolls: A simple one-dimensional elastohydrodynamic model. *Chem. Engng Sci.* **43**, 2673.

Coyle, D. J., Macosko, C. W. & Scriven, L. E. 1986 Film spliting flows in forward roll coating. *J. Fluid Mech.* **171**, 183.

Coyle, D. J., Macosko, C. W. & Scriven, L. E. 1990 Stability of symmetric film-splitting between counter-rotating cylinders. *J. Fluid Mech.* **216**, 437.

Coyne, J. C. & Elrod, H. G. 1970 Conditions for the rupture of a lubricating film. Part I: Theoretical model. *J. Lubrication Tech.* **73**, 451.

Deryagin, B. M. & Levi, S. M. 1959 *Film Coating Theory*. Focal Press Ltd.

Dowson, D. & Higginson, G. R. 1966 *Elasto-Hydrodynamic Lubrication.* Pergamon.

Dowson, D. & Jin, Z. 1989 The influence of elastic deformation upon film thickness in lubricated bearing with low elastic modulus coating. *Proc. 16th Leeds-Lyon Symp. Tribology, Lyon, France*, p. 263.

Fall, C. 1985 A theoretical model of striated film-rupture applied to the cylinder-plane. *J. Tribology* **107**, 419.

Gaskell, P. H., Savage, M. D., Summers, J. L. & Thompson, H. M. 1995 Modelling and analysis of meniscus roll coating. *J. Fluid Mech.* **298**, 113.

Greener, J. & Middleman, S. 1975 A theory of roll coating of viscous and viscoelastic fluids. *Polymer Engng Sci.* **15**, 1.

Greener, J., Sullivan, T., Turner, B. & Middleman, S. 1980 Ribbing instability of a two-roll coater: Newtonian fluids. *Chem. Engng Commun.* **5**, 73.

Hopkins, M. R. 1957 Viscous flow between rotating cylinders and a sheet moving between them. *Br. J. Appl. Phys.* **18**, 442.

Johnson, K. L. 1985 *Contact Mechanics* Cambridge University Press.

Kubota, T. & Scriven, L. E. 1993 Forward roll coating in the runback feed condition. *Proc. IS& T Coating Conf., Boston, USA*, p. 309.

Landau, L. & Levich, B. 1942 Dragging of a liquid by a moving plate. *Acta Physicochim USSR* **17**, 42.

Mill, C. C. & South, G. R. 1967 Formation of ribs on rotating rollers. *J. Fluid Mech.* **28**, 523.

Orchard, S. E. 1962 On surface levelling in viscous liquids and gels. *Appl. Sci. Res.* **11**, 451.

Payne, A. R. & Scott, J. R. 1960 *Engineering Design with Rubber*. Interscience Publishers.

Pearson, J. R. A. 1960 The stability of uniform viscous flow under rollers and spreaders. *J. Fluid Mech.* **7**, 481.

Pitts, E. & Greiller, J. 1961 The flow of thin liquid films between rollers. *J. Fluid Mech.* **11**, 33.

Rabaud, M., Michalland, S. & Couder, Y. 1990 Dynamical regimes of directional viscous fingering: Spatiotemporal chaos and wave propagation. *Phys. Rev. Lett*. **64**, 184.

Saad, Y. & Schultz, M. H. 1986 GMRES: a generalized minimal residue algorithm for solving nonsymetric linear systems. *SIAM J. Sci. Statist. Comput*. **7**, 856.

Savage, M. D. 1977*a* Cavitation in lubrication. Part 1. On boundary conditions and cavity–fluid interfaces. *J. Fluid Mech.* **80**, 743.

Savage, M. D. 1977*b* Cavitation in lubrication. Part 2. Analysis of wavy interfaces. *J. Fluid Mech.* **80**, 757.

Savage, M. D. 1982 Mathematical models for coating process. *J. Fluid Mech.* **117**, 443.

Savage, M. D. 1984 Mathematical model for the onset of ribbing. *AIChE J.* **30**, 999.

Savage, M. D., Gaskell, P. H., Malone, B. & Thompson, H. M. 1992 The relevance of lubrication theory to roll coating. *Proc. AIChE Spring National Meeting, New Orleans,USA*.

Thompson, J. F., Warsi, Z. & Mastin, C. W. 1985 *Numerical Grid Generation, Foundations and Applications.* North-Holland.